

Insight into the Hydrogen Migration Processes Involved in the Formation of Metal-Borane Complexes: The Importance of the Third Arm of the Scorpionate Ligand

Nikolaos Tsoureas, Alex Hamilton, Mairi F. Haddow, Jeremy N. Harvey, A. Guy. Orpen

*and Gareth R. Owen, *†*

The School of Chemistry, University of Bristol, Bristol, BS8 1TS, UK.

Additional Experimental Details

Sodium deuteriotris(7-azaindoly)borate, Na[Tai-d₁]

The solids Na[BD₄] (125 mg, 2.99 mmol) and 7-azaindole (1.56 g, 4.4 eq) were grinded together in a pestle and mortar, and placed in a 50 ml RBF equipped with a Schlenk adaptor. The solid mixture was degassed and heated at 180 °C for 2 hours in a thermostated oil bath under an inert atmosphere (N₂) with stirring. The yellow brown residue was carefully scrapped and washed with hot toluene (3 x 20 mL) and filtered hot. It was then dried under vacuum to give the deuterated ligand. The toluene washings were reduced to approximately half and placed in a -30 °C to give a second crop which was isolated by filtration. Finally the mother-liquor of the second crop was cooled at -80 °C to give a third crop. Combined Yield: 750 mg (65%). ¹H-NMR (δ CD₃CN, 300 MHz): 6.35 (3H, d, ³J_{HH} = 3.30 Hz), 6.90 (3H, dd, ³J_{HH} = 4.76 Hz, ³J_{HH} = 7.87 Hz), 7.23 (3H, dd, ⁴J_{HH} = 1.10 Hz, ³J_{HH} = 3.30 Hz), 7.87 (3H, dd, ⁴J_{HH} = 1.87 Hz, ³J_{HH} = 7.87 Hz), 8.05 (3H, dd, ⁴J_{HH} = 1.65 Hz, ³J_{HH} = 4.76 Hz); ¹H{¹¹B}-NMR (δ CD₃CN, 300 MHz): no extra signals than those observed in the ¹H-NMR; ¹¹B{¹H}-NMR (δ CD₃CN, 96.2 MHz): -7.2 (s); ¹¹B-NMR (δ CD₃CN, 96.2 MHz): -7.2 (s); ¹¹B{¹H}-NMR (δ CD₃CN, 160.4 MHz): -7.2 (t, ¹J_{BD} = 12.7 Hz); ²H-NMR (δ CD₃CN, 76.7 MHz): 5.91 (br s); HRMS (ESI): Calc for [C₂₁H₁₅BDN₆]⁻: 364.1598 Found: 364.1604.

[Ir{ κ^3 -*NNH*-B(D)(azaindolyl)₃}(COD)] (4-d₁)

The synthesis and characterization of **4-d₁** was found to be analogous to that previously reported for **4**.^{S1} Selected data: NMR (δ C₆D₆), ¹B{¹H} (96.2 MHz): 2.1 (s, hhw. = 55 Hz); ¹¹B: 2.1 (s, hhw. = 60 Hz); ²H-NMR (δ C₆D₆, 76.7 MHz) 4.69 (s, br).

[Ir(C₈H₁₂D){ κ^3 -*NNB*-B(azaindolyl)₃}(CO)₂] (5-d₁)

The synthesis and characterization of **5-d₁** was found to be analogous to that previously reported for **5**. Selected data: NMR (δ C₆D₆/C₆H₆), see Figure 2 in manuscript for full assignments. ¹H (500 MHz), 2.27 (1H, m, C₈H₁₂D), 1.90 (2H, m, C₈H₁₂D), 1.86 (1H, m C₈H₁₂D), 1.79 (1H, m, C₈H₁₂D), 1.68 (1H, m, C₈H₁₂D), 1.45 (1H, C₈H₁₂D), 1.26 (1H, C₈H₁₂D), 1.14 (1H, m, C₈H₁₂D), -0.04 (1H, C₈H₁₂D). ¹³C{¹H} (125 MHz), 46.7 (t, ¹J_{CD} = 18.0 Hz), [45.0, 32.0, 29.0, 26.2 (CH₂'s of cyclooctenyl)], 17.4 (Ir-CH). ²H-NMR (76.7 MHz) 1.90 (s, br).

[Ir(C₈H₁₂D){ κ^3 -*NNB*-B(azaindolyl)₃}(CO)] (6-d₁)

The synthesis and characterization of **6-d₁** was found to be analogous to that previously reported for **6**. Selected data: NMR (δ C₆D₆/C₆H₆), see Figure 2 in manuscript for full assignments. ¹H (500 MHz), 2.27 (1H, m, C₈H₁₂D), 2.00 (1H, C₈H₁₂D), 1.90 (1H, m, C₈H₁₂D), 1.67 (3H, m C₈H₁₂D), 1.48 (1H, C₈H₁₂D), 1.30 (1H, C₈H₁₂D), 1.09 (1H, m, C₈H₁₂D), 0.98 (1H, C₈H₁₂D). ¹³C{¹H} (125 MHz), [41.2, 29.3, 28.8, 24.4 (CH₂'s of cyclooctenyl)], 27.5 (t, ¹J_{CD} = 17.6 Hz), 22.4 (Ir-CH). ²H-NMR (76.7 MHz) 1.30 (s, br).

[Li(THF)₂][BD₃Ph]

¹H-NMR (δ C₆D₆, 300 MHz): 1.26 (8H, m, CH₂), 3.56 (8H, m, CH₂), 7.27 (1H, ddt, ⁴J_{HH} = 1.47 Hz, ⁴J_{HH} = 1.28 Hz, ³J_{HH} = 7.34 Hz), 7.45 (2H, t, ³J_{HH} = 7.34 Hz), 7.92 (2H, br s); ¹¹B{¹H}-NMR (δ C₆D₆): -27.9 (sept., ¹J_{BD} = 11.76 Hz); ¹¹B-NMR (δ C₆D₆): -27.9 (dsept., ¹J_{BD} = 11.76 Hz, ³J_{BH} = 4.76 Hz); ²H-NMR (δ C₆D₆, 76.74 MHz): -5.02 (br q., ¹J_{BD} = 11.76 Hz).

Lithium deuteriophenylbis(7-azaindoly)borate, Li[^{Ph}Bai-d₁]

The synthesis and characterization of Li[^{Ph}Bai-d₁] was found to be analogous to that previously reported for Li[^{Ph}Bai].^{S2} ¹¹B{¹H}-NMR (δ CD₂Cl₂, 160.38 MHz): -8.7, -3.9 (t, ¹J_{BD} = 22 Hz); ²H-NMR (δ CD₂Cl₂, 76.74 MHz): 5.02, 4.69 (br s).^{S3}

[Ir{κ³-NNH-(Ph)(D)B(azaindoly)₂}(COD)] (15-d₁)

The synthesis and characterization of **15-d₁** was found to be analogous to that previously reported for **15**.^{S2} Selected data: NMR (δ C₆D₆), ¹¹B{¹H} (160.4 MHz), -0.5 (s, hhw. = 95 Hz); ²H-NMR (76.7 MHz) 3.54 (s, br).

Reaction mixture involving [Ir{κ³-NNH-(Ph)(D)B(azaindoly)₂}(COD)] (15-d₁) and CO

Selected data for: [Ir(η¹-C₈H₁₂D){κ³-NNB-(Ph)B(azaindoly)₂}(CO)₂] (**16-d₁**), ¹H-NMR (500 MHz)^{S4} δ(C₆D₆): 5.65 (1H, m, CH=CH), 5.52 (1H, m, CH=CH), [2.08 (m, 1H), 1.93 (m, 2H), 1.85 – 1.64 (m, 4 H), 1.52 (m, 1H), 1.09 (m, 1H), many of these signals overlap with those for **18-d₁**, total 9H, C₈H₁₂D], -0.21 (1H, br. s, β-hydrogen, IrC₈H₁₂D); ¹³C{¹H}-NMR (125 MHz) δ(C₆D₆): 45.6 (t, ¹J_{CD} = 18.0 Hz), 44.6, 31.9, 29.6, 26.7 (CH₂s of cyclo-octenyl), 18.3 (Ir-CH); [Ir(H){κ³-NNB-(Ph)B(azaindoly)₂}(CO)₂] (**17-d₁**), ¹H-NMR (500 MHz) δ(C₆D₆): -14.5 (s, Ir-H, this signal showed a trace of hydrogen incorporation at this site after 15 mins). ²H-NMR (δ C₆H₆, 76.7 MHz) -14.5 (s, Ir-D). [Ir(σ¹,η²-C₈H₁₂D){κ³-NNB-(Ph)B(azaindoly)₂}(CO)] (**18-d₁**): ¹H-NMR (500 MHz) δ(C₆D₆): 3.89 (1H, m, CH=CH), 3.28 (1H, m, CH=CH), [2.72 (m, 1H), 2.42 (m, 1H), 2.08 (m, 1H), 1.85 – 1.64 (m, 5 H), 1.52 (m, 1H), 1.40 (m, 1H), many of these signals overlap with those for **16-d₁**, total 10H, C₈H₁₂D], ¹³C{¹H}-NMR (125 MHz) δ(C₆D₆): 59.7 (CH=CH), 49.8 (CH₂), 46.1 (CH=CH), 36.3 (t, ¹J_{CD} = 19.1 Hz), 29.8, 27.3, 27.0 (CH₂s of cyclo-octenyl), 15.7 (Ir-CH).

The integration of the signals in the ¹H NMR of the reaction mixture changed over time suggesting deuterium scrambling and a dynamic process involving the interconversion between the species in the mixture. Accurate determination of this process was precluded by the fact that the ratio of the products also changed over time. Nevertheless a ¹H NMR spectrum of the mixture after 5 days revealed the presence of approximately equal amounts of **17** and **17-d₁** (totaling 25% of the mixture with respect to

16, **16-d₁**, **18** and **18-d₁**). There were a number of changes in the region of the spectrum between 1.80 and -0.25 ppm. New signals appeared at 1.40 and 1.29 ppm. These were previously observed in the spectra for **16** and **18**. At the same time, the integration of the signals between 1.85 – 1.64 ppm and at 1.09 and -0.25 ppm all reduced in intensity. This evidence suggests that the deuterium and hydrogen atoms are being exchanged via a series of β -hydride elimination and migratory insertion steps.

Figures of selected NMR spectra

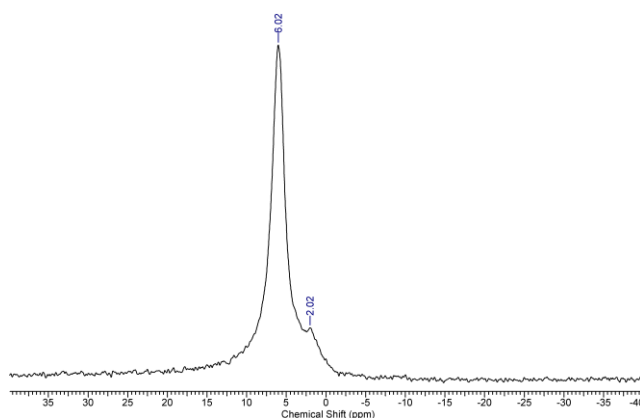


Figure S1 – $^{11}\text{B}\{^1\text{H}\}$ NMR spectrum of the reaction involving **15** with CO (only two complexes are apparent in the spectrum although the corresponding ^1H NMR spectrum is consistent with the presence of the three complexes, **16**, **17** and **18**).

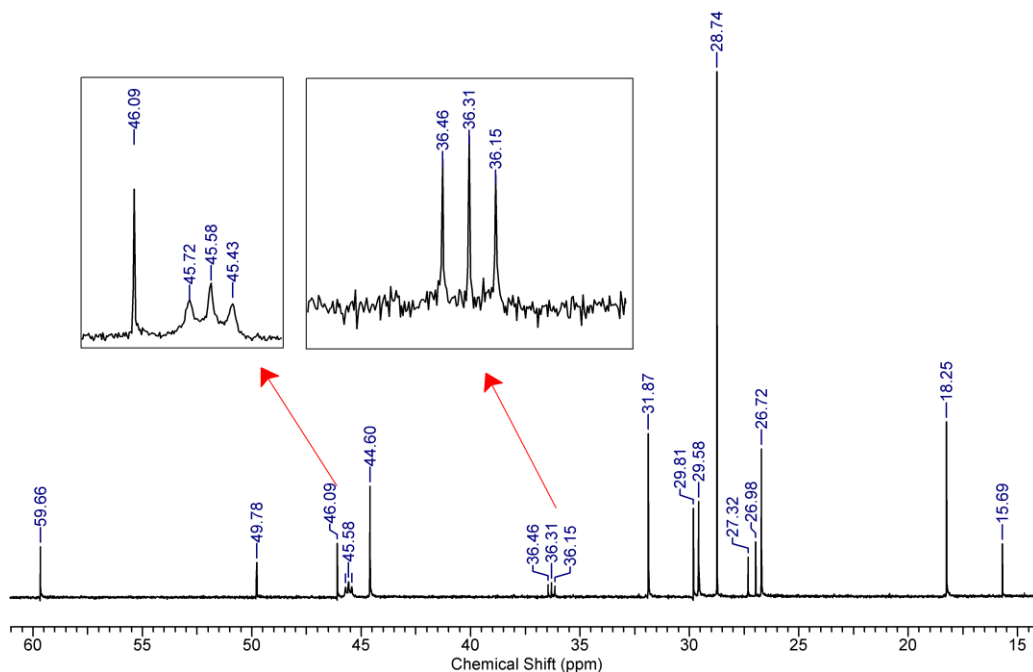


Figure S2 – The aliphatic region of the $^{13}\text{C}\{^1\text{H}\}$ NMR spectrum of the reaction involving **15-d₁** with CO (C_6D_6). Initially, deuterium incorporation is observed at 45.6 ppm and 36.3 ppm, identified as the β -positions on $[\text{Ir}(\sigma^1\text{-C}_8\text{H}_{12}\text{D})\{\kappa^3\text{-NNB-(Ph)B(azaindoly)}_2\}(\text{CO})]$ (**16-d₁**) and $[\text{Ir}(\sigma^1, \eta^2\text{-C}_8\text{H}_{12}\text{D})\{\kappa^3\text{-NNB-(Ph)B(azaindoly)}_2\}(\text{CO})]$ (**18-d₁**), respectively. The signal at 28.7 ppm corresponds to the methylene units in the free COD formed during the reaction.

Computational details

All the DFT calculations were performed using the program Jaguar v6.0 with the graphical interface Maestro v5.1. Geometry optimisation for all species was carried out using the B3PW91 hybrid functional with the 6-31G* basis set on all atoms except iridium; for the latter, the Los Alamos relativistic ECP and associated LACV3P was used. The LACV3P basis is a triple zeta valence basis set which was developed for use with Los Alamos ECP and the Jaguar program. Zero point energy corrections were calculated from frequency calculations for each intermediate using model calculations where the COD ring was replaced with 1 or 2 ethene ligands or ethyl depending on coordination. A correction for dispersion interactions was obtained by carrying out B3LYP and B3LYP-D calculations (on the non-model systems) using the ORCA program package. The dispersion corrected B3LYP-D

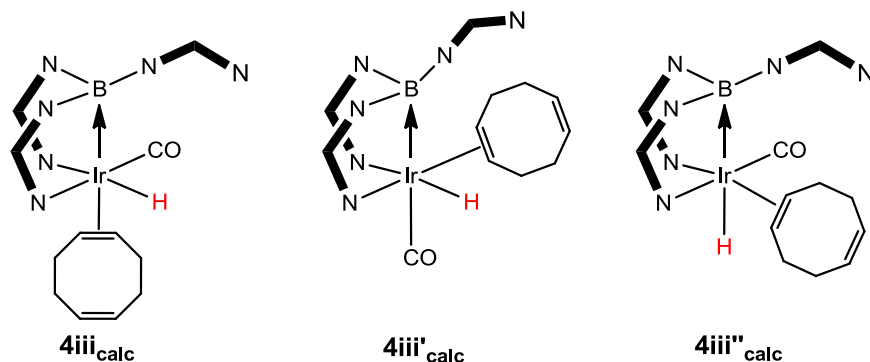
functional as suggested by Grimme^{S5} together with the all electron TZV_P basis set on iridium, and the SV (on H's) and SVP (all other atoms) basis sets was used. The B3LYP and B3LYP-D energies were used to cross-check the B3PW91 results (and shows good agreement; results not reported here) and also to determine the dispersion correction. This was then added to the B3PW91 results to give a dispersion corrected "B3PW91-D" result as discussed in the main text. All reported energies are relative electronic energies, including the correction for zpe from the model complex calculations and the dispersion correction.

For the known structures, **4** and **6** the crystal structure geometry was used as the calculation input geometry. Complexes along the reaction pathway can adopt different structural isomers, for examples complex **4iii** can adopted 3 different isomers, see Figure S3. The relative energies of the different isomers was calculated using the model complexes (where COD has been replace with 1 or 2 ethene ligands, depending on coordination, and octenyl has been replaced with ethyl). The uncoordinated azaindole group seemed to adopt 1 of 2 different conformations involving M–B–N–C torsion angles of $\sim 180^\circ$ or $\sim -80^\circ$. These conformations have been explored for the lowest energy isomers of each complex to ensure the low energy geometries are used, calculations undertaken on the full (COD) complex. The lowest energy conformation of the **Tai** ligand (in structure **4iii_{calc}**) is where the uncoordinated azaindolyl group is rotated through an angle of -73.9° with respect to the Ir–B vector, as measured by the Ir–B–N–C torsion angle.

Further computational investigations

Alternative isomers of **4iii**

There are two alternative structural isomers of **4iii_{calc}** in which the COD, CO and H ligand occupy different coordination sites relative to the B(azaindolyl)₃ ligand, as shown in Figure S3. The relative energies of these three isomers were calculated. Structure **4iii_{calc}** was found to be the lowest energy isomer. Structures **4iii'_{calc}** and **4iii''_{calc}** were found to be 14.9 kcal mol⁻¹ and 8.9 kcal mol⁻¹ less stable than **4iii_{calc}** (relative energies, not including dispersion correction).



E_{rel} (kcal mol ⁻¹)	0.0	14.9	8.9
--------------------------------------------	-----	------	-----

Figure S3 – Possible structural isomers of **4iii_{calc}** and their associated relative energies in kcal mol⁻¹

Potential κ^4 -NNBN coordination mode for **Tai**

As noted in the main text the **Tai** ligand has the potential to coordinate with a κ^4 -NNBN coordination mode. To determine whether this coordination mode is utilised in the reaction mechanism, calculations of possible structures contain the κ^4 -NNBN motif were computed relative to the **4_{calc}**. Three possible structures were calculated, the square based pyramidal complex [Ir{ κ^4 -NNBN-B(azaindoly)₃}(C₈H₁₃)] (**A**) and two isomeric octahedral complexes containing one carbonyl ligand [Ir{ κ^4 -NNBN-B(azaindoly)₃}(CO)(C₈H₁₃)] (**B** and **C**). In the latter two complexes the carbonyl ligand occupies the site cis (**B**) or trans (**C**) to the borane ligand. The calculated free energies of **A** to **C** were -5.0 kcal mol⁻¹, -23.8 kcal mol⁻¹ and -7.2 kcal mol⁻¹, respectively. While all three structures are lower in energy than **4_{calc}**, they are all higher in energy than complex **5** or **6** (c.f. -42.2 kcal mol⁻¹ and -30.3 kcal mol⁻¹).

Inter-conversion between **5** and **6**

As highlighted in the main article, there is a 24.4 kcal mol⁻¹ difference in energy between the calculated structures **5_{calc}** and **6_{calc}** in the potential energy calculations and only a 11.9 kcal mol⁻¹ difference in terms of free energy. The calculated structures are provided in Figure S4.

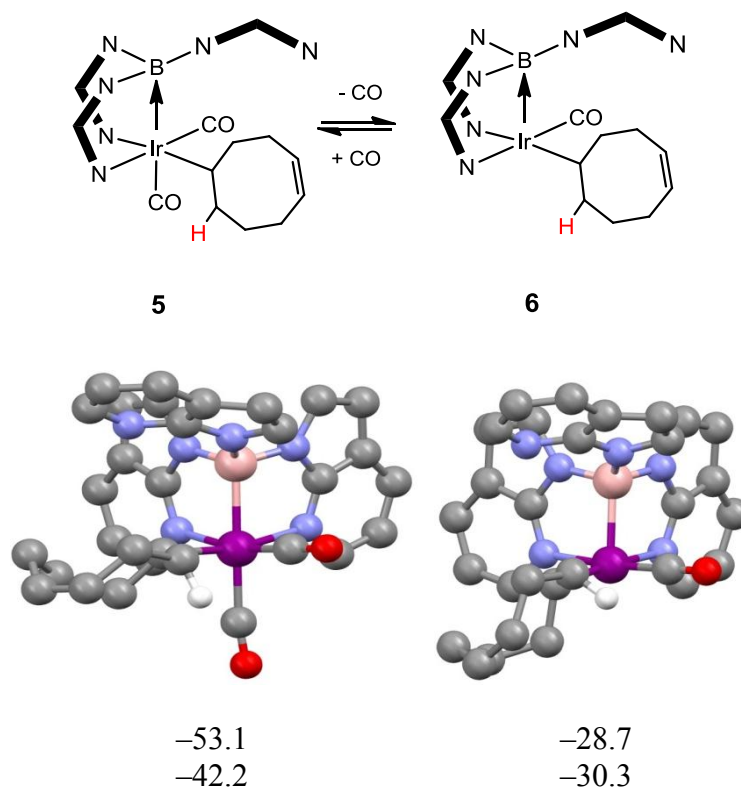


Figure S4 – Schematic diagrams for complexes **5** and **6** and their respective calculated geometries (**5_{calc}** and **6_{calc}**). Their energies relative to the starting complex **4_{calc}** are given below each structure in units of kcal mol⁻¹. All hydrogen atoms (except migrating hydrogen) have been omitted for clarity.

Table S1 – Selected bond lengths (Å), angles and torsion angles (°) for the calculated structures in this study.

	4_{calc}	4i_{calc}	4ii_{calc}	TS₁	4iii_{calc}	TS₂	5_{calc}	6_{calc}
Ir-N	2.17 / 2.12	2.11	2.14 / 2.18	2.14 / 2.18	2.14 / 2.22	2.16 / 2.08	2.12 / 2.23	2.18 / 2.26
Ir-H	1.94	1.84	1.92	1.63	1.59	1.71	-	-
Ir-B	2.98	3.05	2.96	2.41	2.21	2.24	2.28	2.21
B-H	1.25	1.31	1.26	1.68	2.54	-	-	-
Ir-C	-	-	-	-	-	2.21	2.17	2.08
Ir-C=C	2.02 / 1.98	2.06 / 2.07	2.00	2.05	2.31	2.14	-	-
Ir-CO	-	1.90	1.83	1.84	1.84	1.84	1.86 / 1.98	1.84
B-Ir-H	-	-	17.0	44.3	82.0	92.7	-	-
Ir-H-B	137.2	151.1	136.5	-	-	-	-	-
OC-Ir-H	-	-	93.7	91.3	88.0	-	-	-
N-Ir-N	86.4	-	86.3	88.2	87.8	88.3	86.8	86.8
B-Ir-C=C	-	-	131.1	152.7	171.4	145.8	-	-
C=C-Ir-C=C	86.9	85.5	-	-	-	-	-	-
B-Ir-C	-	-	-	-	-	162.3	89.0	104.9
Ir-B-N-C	178.8	174.1	179.1	173.9	-73.9	-66.1	-90.1	-84.8

Table S2 – Computational potential (ΔE) and free energy (ΔG_{298}) results. All data is ZPE corrected, the B3PW91 calculations undertaken with Jaguar and the B3LYP/B3LYP-D calculations undertaken with ORCA. The D correction used for B3PW91 was taken from the B3LYP results.

	B3PW91 6-31G* (Ir) (ΔE)	B3PW91 (D) 6-31G* (Ir) (ΔE)	B3PW91 6-31G* (Ir) (ΔG_{298})	B3PW91 (D) 6-31G* (Ir) (ΔG_{298})
4_{calc}	0.0	0.0	0.0	0.0
4i_{calc}	-12.3	-16.4	-2.0	-6.1
4ii_{calc}	-17.0	-14.8	-18.2	-16.0
TS₁	-4.9	-5.1	-5.5	-5.7
4iii_{calc}	-19.7	-17.5	-21.6	-19.4
TS₂	-2.9	4.3	0.3	1.7
5_{calc}	-42.2	-53.1	-31.3	-42.2
6_{calc}	-27.7	-28.7	-29.3	-30.3

Crystallography

The data for **5**, **6**, **13** and **20** were collected on a Bruker Kappa Apex II CCD detector diffractometer with a fine-focus sealed tube MoKa radiation source and a Cryostream Oxford Cryosystems low temperature device. The programs used for control and integration were APEXII, SAINT v7.34A and XPREP v2005/4.^{S6} The crystals were mounted on a glass fibre with silicon grease. All solutions and refinements were performed using the Bruker ShelXTL software and all software packages within.^{S7} All non-hydrogen atoms were refined using anisotropic thermal parameters, and hydrogen atoms were added using a riding model. This is with the exception of H100 in complex **20** which was located in the difference map. Preliminary details concerning the structures of **6** and **11** have been reported^{S8} and they have previously been deposited in the Cambridge Structural Database [CCDC 713892 (**6**) and CCDC 713893 (**11**). The data collection parameters and refinement information are presented in Table S4 in the supporting information. Full details of the anisotropic parameters, bond lengths and (torsion) angles for complexes **13** and **20** are available from the cif file. This information is free of charge. Figures 1, 3, 4 and 5 in the manuscript have been generated using ORTEP and POV-Ray software.^{S9}

Additional selected bond distances (Å) and angles (°) highlighting the conformation of the cyclooctenyl group in complexes 6, 11 and 13

Complex **6** (see Figure 1 in manuscript): C₂₃–C₂₄ 1.567(7), C₂₄–C₂₅ 1.524(7), C₂₅–C₂₆ 1.549(7), C₂₆–C₂₇ 1.497(8), C₂₇–C₂₈ 1.331(8), C₂₈–C₂₉ 1.512(8), C₂₉–C₃₀ 1.542(7), C₃₀–C₂₃ 1.527(7), C₂₃–C₂₄–C₂₅ 116.5(4), C₂₄–C₂₅–C₂₆ 115.1(4), C₂₅–C₂₆–C₂₇ 111.4(5), C₂₆–C₂₇–C₂₈ 123.6(6), C₂₇–C₂₈–C₂₉ 124.7(6), C₂₈–C₂₉–C₃₀ 114.8(4), C₂₉–C₃₀–C₂₃ 116.9(5), C₃₀–C₂₃–C₂₄ 112.9(5), C₂₃–C₂₄–C₂₅–C₂₆ –54.7(7), C₂₄–C₂₅–C₂₆–C₂₇ –51.8(7), C₂₅–C₂₆–C₂₇–C₂₈ 88.2(7), C₂₆–C₂₇–C₂₈–C₂₉ 6.0(9), C₂₇–C₂₈–C₂₉–C₃₀ –84.1(7), C₂₈–C₂₉–C₃₀–C₂₃ 73.8(7), C₂₉–C₃₀–C₂₃–C₂₄ –70.7(6), C₃₀–C₂₃–C₂₄–C₂₅ 102.5(6), B₁–Ir₁–C₂₃–C₂₄ 163.6(3), B₁–Ir₁–C₂₃–C₃₀ –75.0(4).

Complex **11** (see Figure 2 in manuscript): C₂₂–C₂₃ 1.537(4), C₂₃–C₂₄ 1.536(4), C₂₄–C₂₅ 1.529(4), C₂₅–C₂₆ 1.507(5), C₂₆–C₂₇ 1.338(5), C₂₇–C₂₈ 1.484(4), C₂₈–C₂₉ 1.542(5), C₂₉–C₂₂ 1.541(4), C₂₂–C₂₃–C₂₄ 115.4(2), C₂₃–C₂₄–C₂₅ 115.1(3), C₂₄–C₂₅–C₂₆ 113.9(3), C₂₅–C₂₆–C₂₇ 124.6(3), C₂₆–C₂₇–C₂₈ 124.2(3), C₂₇–C₂₈–C₂₉ 112.2(3), C₂₈–C₂₉–C₂₂ 114.2(3), C₂₉–C₂₂–C₂₃ 112.6(3), C₂₂–C₂₃–C₂₄–C₂₅ 77.1(4), C₂₃–C₂₄–C₂₅–C₂₆ –73.4(3), C₂₄–C₂₅–C₂₆–C₂₇ 81.0(4), C₂₅–C₂₆–C₂₇–C₂₈ –3.4(5), C₂₆–C₂₇–C₂₈–C₂₉ –91.9(4), C₂₇–C₂₈–C₂₉–C₂₂ 53.0(4), C₂₈–C₂₉–C₂₂–C₂₃ 51.2(3), C₂₉–C₂₂–C₂₃–C₂₄ –105.3(3), B₁–Ir₁–C₂₂–C₂₃ –140.5(3), B₁–Ir₁–C₂₂–C₂₉ 89.8(3).

Complex **13** (see Figure 3 in manuscript): C₂₃–C₂₄ 1.531(6), C₂₄–C₂₅ 1.559(6), C₂₅–C₂₆ 1.491(8), C₂₆–C₂₇ 1.310(9), C₂₇–C₂₈ 1.497(9), C₂₈–C₂₉ 1.532(8), C₂₉–C₃₀ 1.541(6), C₃₀–C₂₃ 1.548(6), C₂₃–C₂₄–C₂₅ 115.7(4), C₂₄–C₂₅–C₂₆ 111.1(4), C₂₅–C₂₆–C₂₇ 125.0(6), C₂₆–C₂₇–C₂₈ 125.8(6), C₂₇–C₂₈–C₂₉ 116.8(4), C₂₈–C₂₉–C₃₀ 115.4(5), C₂₉–C₃₀–C₂₃ 114.9(4), C₃₀–C₂₃–C₂₄ 112.8(3), C₂₃–C₂₄–C₂₅–C₂₆ 55.0(6), C₂₄–C₂₅–C₂₆–C₂₇ –89.8(7), C₂₅–C₂₆–C₂₇–C₂₈ –4.2(9), C₂₆–C₂₇–C₂₈–C₂₉ 78.7(8), C₂₇–C₂₈–C₂₉–C₃₀ –69.8(7), C₂₈–C₂₉–C₃₀–C₂₃ 76.2(6), C₂₉–C₃₀–C₂₃–C₂₄ –105.0(5), C₃₀–C₂₃–C₂₄–C₂₅ 48.2(5), B₁–Ir₁–C₂₃–C₂₄ 92.3(3), B₁–Ir₁–C₂₃–C₃₀ –136.7(3).

Table S3 – Crystallographic data and refinement parameters for **6**, **11**, **13** and **20**

Compound	Complex 6	Complex 11	Complex 13	Complex 20
Colour, habit	pale yellow block	colourless needle	colourless block	colourless block
Size/mm	0.18×0.08×0.04	0.34×0.04×0.04	0.36×0.16×0.08	0.303×0.231×0.18
Empirical Formula	C ₃₀ H ₂₈ BIrN ₆ O	C ₄₆ H ₄₅ BIrN ₇ O	C ₃₆ H ₃₉ BIrN ₆ O ₄ P	C ₂₈ H ₂₄ BIrN ₄ O
M	691.59	914.90	853.71	635.52
Crystal system	monoclinic	monoclinic	monoclinic	trigonal
Space group	<i>P</i> 2 ₁ / <i>n</i>	<i>P</i> 2 ₁	<i>P</i> 2 ₁ / <i>c</i>	<i>R</i> $\bar{3}$
<i>a</i> /Å	9.2778(4)	9.75060(10)	15.3955(8)	18.4965(4)
<i>b</i> /Å	17.5888(7)	14.8856(2)	15.0565(8)	18.4965(4)
<i>c</i> /Å	15.9156(6)	14.0027(2)	33.9742(17)	38.7777(7)
α /°	90.00	90.00	90.00	90.00
β /°	93.999(2)	104.9800(10)	103.987(3)	90.00
γ /°	90.00	90.00	90.00	120.00
<i>V</i> /Å ³	2590.87(18)	1963.33(4)	7641.8(7)	11489.2(4)
<i>Z</i>	4	2	8	18
μ /mm ⁻¹	5.190	3.447	3.581	5.257
T/K	100	173	100	100
$\theta_{\text{min,max}}$	1.73,27.48	3.24,30.57	1.36,30.55	3.30,30.61
Completeness	0.998 to θ = 27.48°	0.986 to θ = 30.57°	0.997 to θ = 30.55°	0.997 to θ = 27.50°
Reflections: total/independent	23859/5925	30024/11606	285993/23344	70035/6032
<i>R</i> _{int}	0.0637	0.0363	0.0569	0.0612
Final <i>R</i> 1 and <i>wR</i> 2	0.0385, 0.0897	0.0252, 0.0505	0.0425, 0.1034	0.0213, 0.0436
Largest peak, hole/eÅ ⁻³	1.636, -1.282	0.748, -0.968	2.949, -4.808	0.694, -0.451
ρ_{calc} /g cm ⁻³	1.773	1.548	1.484	1.653

References

- S1 Owen, G. R.; Tsoureas, N.; Hamilton, A.; Orpen, A. G. *Dalton Trans.*, **2008**, 6039.
- S2 Tsoureas, N.; Bevis, T.; Butts, C. P.; Hamilton, A.; Owen, G. R. *Organometallics*, **2009**, *28*, 5222.
- S3 As found in Li[^{Ph}Bai], there were two found in solution, one is consistent with [Li{Ph(H)B(azaindoly)}₂]₂ and the other [Li•THF_{*n*}][^{Ph}Bai] – see reference S2 and Owen, G. R.; Tsoureas, N.; Hope, R. F.; Kuo, Y.-Y.; Haddow, M. F. *Dalton Trans.* **2011**, *40*, 5906.

S4 The aromatic region of the spectra involving the mixture **16-d₁**, **17-d₁** and **18-d₁** involves 39 chemical environments (45 H in total) and was rather complicated. We were therefore unable to assign these signals with any degree of confidence. For the same reason the proton assignments given for the aliphatic region of the spectra are tentative.

S5 (a) Grimme, S. *J. Comp. Chem.* **2004**, *25*, 1463. (b) Grimme, S. *J. Comp. Chem.* **2006**, *27*, 1787.

S6 Bruker-AXS, **2007**; Bruker-AXS, **2005**.

S7 G. M. Sheldrick, *Acta Crystallogr., Sect. A: Found. Crystallogr.*, **2008**, *64*, 112.

S8 Tsoureas, N.; Haddow, M. F.; Hamilton, A.; Owen, G. R. *Chem. Commun.* **2009**, 2538.

S9 (a) ORTEP-3 for Windows v2.02; Farrugia, L. J. *J. Appl. Cryst.* **1997**, *30*, 565. (b) POV-Ray for Windows v3.6.2, Persistence of Vision Pty. Ltd., 2004, computer software, retrieved from <http://www.povray.org/download/>.